Synthesis of Lithium-Aluminum Layered Double Hydroxide Adsorbent from Aluminum Waste to Create a More Environmentally Friendly Process for Recovering Lithium in Brine

Salafudin Salafudin[1], Agus Prasetya[1,2*], I Wayan Warmada[2,3], and Himawan Tri Bayu Murti Petrus[1,2]

[1]*Department of Chemical Engineering, Faculty of Engineering, Universitas Gadjah Mada, Jl. Grafika No. 2, Yogyakarta 55281, Indonesia*

[2]*Unconventional Geo-Resources Research Group (UGRG), Faculty of Engineering, Universitas Gadjah Mada, Jl. Grafika No. 2, Yogyakarta 55281, Indonesia*

[3]*Department of Geological Engineering, Faculty of Engineering, Universitas Gadjah Mada, Jl. Grafika No. 2, Yogyakarta 55281, Indonesia*

** Corresponding author:*

email: aguspras@ugm.ac.id

Received: June 11, 2024
Accepted: April 8, 2025

DOI: 10.22146/ijc.97024

Abstract: *All countries pledged to strive to limit global warming. The implementation of renewable energy must be accelerated. One of the most essential components of renewable energy is lithium-ion batteries. The surging demand for lithium necessitates new technologies for direct recovery from brine. One of the most promising methods is adsorption. Because of its advantages, lithium-aluminum layered double hydroxides have started their application on a commercial scale. This research uniquely explores the synthesis of lithium adsorbent from aluminum waste, an approach that is both cost-effective and environmentally sustainable. The reaction behavior was studied, including the rate of hydrogen gas production and the co-precipitation process. The quality of the product was assessed by its adsorption capacity and characterization. The synthesis of lithium adsorbent was successfully performed through two-step processes, with the reaction kinetics studied at temperatures between 30 and 60 °C. XRD and FTIR results confirmed the adsorbent product. The adsorbent worked well for synthetic brine with 39–1350 ppm lithium concentration and adsorption capacity until 6.7 mg lithium ion per g of adsorbent. These findings contribute to the development of sustainable technologies for lithium extraction and can be applied to improve industrial lithium recovery processes.*

Keywords: *lithium; aluminum; waste; brine; layered double hydroxides*

■ INTRODUCTION

The use of fossil energy has led to significant CO_2 emissions, contributing to global warming and related challenges [1-2]. Accelerating renewable energy implementation demands efficient energy storage systems [3]. As the vital part of renewable energy, lithium-ion batteries are known for their high energy density, long-lasting and reliable performance [4-5]. Lithium-ion batteries are expected to account for about five million tons of annual demand by 2050, with an estimated market value of about half a trillion [6]. This rising demand for lithium drives the need for improved and more sustainable recovery methods, especially from low-grade sources [7].

Adsorption using lithium-aluminum layered double hydroxides (LDHs) is a promising method for lithium recovery due to its eco-friendly properties and high selectivity for lithium ions [8-10]. Traditional commercial lithium recovery techniques such as solvent extraction, precipitation, and membrane-based processes, typically require significant chemical inputs, generate hazardous by-products, and have high capital and operating costs. Unlike them, the Li/Al LDH approach utilizes industrial aluminum waste as a raw material. This not only offers a cost-effective solution

but also reduces environmental impact by minimizing secondary pollution. Additionally, while commercial methods often involve multiple purification stages that drive up costs and energy consumption, the Li/Al LDH synthesis repurposes aluminum waste, turning it into a valuable resource. This process further reduces chemical usage and carbon footprint, making lithium recovery more economically viable and environmentally sustainable [11-13].

The crystal's layered structure consists of the mineral gibbsite (γ-$Al(OH)_3$), which offers exceptional selectivity for lithium ions. Its minute hexagonal cavities are capable of accommodating exclusively positive ions, such as H^+ and Li^+ [14]. In the adsorption process, lithium ions enter these cavities while chloride ions maintain the charge balance between the layers [11-12,15]. The synthesis of Li/Al based crystal typically involves reactions such as in Eq. 1–6 [16-18]:

$$2NaOH_{(aq)} + 2Al_{(s)} + 6H_2O \rightarrow 2NaAl(OH)_{4(aq)} + 3H_{2(g)} \quad (1)$$

$$2Al_{(s)} + 3H_2O \rightarrow Al_2O_{3(s)} + 3H_{2(g)} \quad (2)$$

$$2NaOH_{(aq)} + Al_2O_{3(s)} + 3H_2O \rightarrow 2NaAl(OH)_{4(aq)} \quad (3)$$

$$NaAl(OH)_{4(aq)} \rightarrow NaOH_{(aq)} + Al(OH)_{3(aq)} \quad (4)$$

$$LiCl_{(aq)} + 2Al(OH)_{3(s)} \rightarrow LiCl{\cdot}Al_2(OH)_{6(s)} \quad (5)$$

$$2NaAl(OH)_{4(aq)} + LiCl_{(aq)} \rightarrow 2NaOH + LiCl{\cdot}Al_2(OH)_{6(s)} \quad (6)$$

Given that the majority of researchers employed analytical-grade compounds to synthesize Li/Al LDH adsorbents, there is limited knowledge about using aluminum waste as a precursor. Additionally, the reaction pathways for hydrogen formation from flat aluminum solids require further elucidation, and the control step that governs the kinetics remains partially understood. There is a pressing need to develop a low-cost, eco-friendly Li/Al LDH adsorbent. Consequently, a manufacturing technology that utilizes waste aluminum to synthesize Li/Al LDHs can address cost and environmental concerns. The objective of this research is to synthesize Li/Al LDH adsorbent from aluminum waste through a two-step reaction. The reaction behavior was investigated, including hydrogen gas production kinetic, and evaluated the product quality through adsorption, XRD, and FTIR characterization.

■ EXPERIMENTAL SECTION

Materials

The majority of the chemical substances utilized were of analytical grade, with the exception of the aluminum waste from a bakery. The following substances were employed: distilled water, NaOH, LiCl, anhydrous $MgCl_2$, and HCl. With the exception of distilled water, the chemical substances utilized were obtained from Merck, Germany. The choice of aluminum foil waste provides high-purity aluminum, a cost-effective and environmentally sustainable option for synthesizing Li/Al LDHs. The selection of experimental conditions, such as NaOH concentration and the reaction temperature, is based on previous research that studied the hydrogen formation reaction with aluminum dross raw materials [17].

Instrumentation

The following instruments were employed: laboratory glassware (Pirex Iwaki), analytical balance, universal model Oven (Memmert UN 30), FTIR IR-Spirit (Serial No A224158), X-ray fluorescence (XRF, NEX QC), atomic absorption spectroscopy (AAS, Type S4 AA System, Thermo Electron Corporation). The Li/Al LDH powder was characterized using XRD and FTIR spectroscopy. XRD was also employed to characterize the aluminum foil waste. The results were analyzed qualitatively to confirm the phase purity and structural integrity of the crystals.

The synthesis of the Li/Al based adsorbent was accomplished through a two-step reaction. Aluminum waste was converted into $NaAl(OH)_4$ solution and hydrogen gas in a batch reactor equipped with a temperature controller and gas reservoir. The reaction involved the reaction of aluminum with NaOH solution, and the produced gas was measured using the water displacement, as shown in Fig. 1. The experimental setup is designed to capture hydrogen gas efficiently. In the subsequent step, the adsorbent was synthesized by implementing simple batch reactors equipped with a temperature-regulated water bath. The experimental

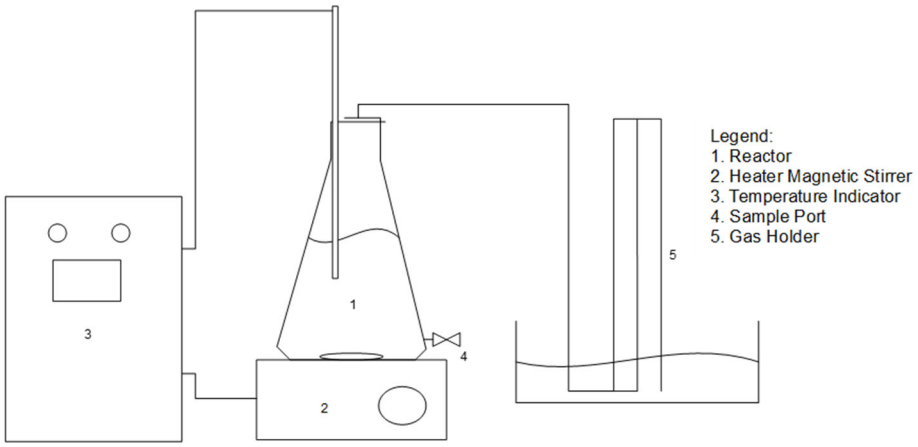

Fig 1. Reactor for first step reaction to produce hydrogen from aluminum waste

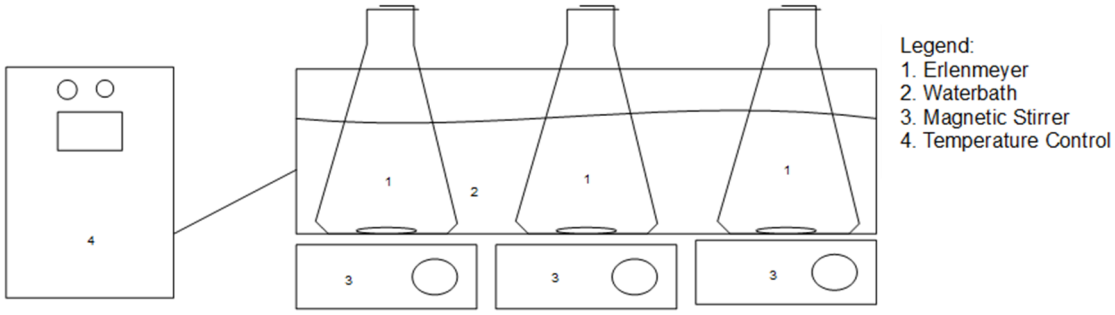

Fig 2. Experimental rig of the second step reaction and adsorption

apparatus employed for this stage, which concurrently evaluated the adsorption efficacy of the Li/Al LDH in batch adsorption, is depicted in Fig. 2.

Procedure

Li/Al LDHs synthesis

The procedure for synthesizing lithium adsorbent was carried out in two steps: conversion of aluminum waste to $NaAl(OH)_4$ and co-precipitation of Li/Al LDHs.

Conversion of aluminum waste to $NaAl(OH)_4$. The aluminum foil waste was thoroughly cleansed and cut into 0.5×0.5 cm^2 fragments to ensure a consistent surface area for reaction. As much as 1 g of aluminum waste was reacted with 100 mL of NaOH solution at concentrations ranging from 0.5 to 2 M, and temperatures from 30 to 60 °C. The reaction was monitored by recording hydrogen gas production. After the reaction was complete, the slurry was filtered to separate solid by-products (primarily Al_2O_3) from the filtrate ($NaAl(OH)_4$). The solids were dried at 105 °C overnight before recording the final weight.

Co-precipitation of Li/Al LDHs. The co-precipitation reaction was carried out using the filtrate from the aluminum waste reaction mixed with 0.5 M NaOH solution at 30 °C. The stoichiometric ratio of Li/Al reactants was maintained at 2. The Li/Al-based crystal formation rate was monitored by analyzing the change in Li concentration during the reaction using AAS. A study was conducted to examine the impact of pH (9–11) and temperature (30–60 °C) on the rate of co-precipitation reaction.

Li/Al LDHs performance

The crystal adsorbent was filtrated, followed by rinsing with a 96% alcohol solution at an L/S ratio of 1. After drying at 60 °C, the adsorbent was activated through a water washing process at L/S = 40 for 2 h to enhance its adsorption efficiency. This step activation step ensures the adsorbent is fully prepared for optimal performance in brine solution. For the adsorption tests, synthetic brine with varying concentrations of Li^+ (39–1067 ppm) and $MgCl_2$ (0–2 M, or 0–48610 ppm) was utilized.

In a controlled environment, 1 g of activated adsorbent was meticulously amalgamated with brine, exhibiting an L/S ratio of 20, under isothermal conditions for a duration of 4 h. After attaining equilibrium, the resultant slurry underwent filtration, and the filtrate was subjected to rigorous analysis using AAS. The data on equilibrium concentration and adsorption capacity was fitted to several adsorption equilibrium models to study the adsorption conditions.

Data analysis

Surface reaction as rate limiting step. The hydrogen gas production rate data were used to fit a kinetic model for the heterogeneous reaction between NaOH solution and aluminum foil. Heterogeneous reactions involve serial steps: mass transfer processes and chemical reactions [19]. This reaction follows the shrinking core model; therefore, the limiting step is the surface reaction or mass transfer [20]. Given that the solid by-product (Al_2O_3) was small and Eq. (3) was very slow, only Eq. (1) and (2) were involved in the first stage.

In heterogeneous solid-phase reactions, the conventional unit of measurement is moles per unit area per unit time. However, given that the solid is present in the form of sheets, it can be posited that the total surface area of the solid remains constant during the reaction. To account for this, the reaction rate can be adjusted by multiplying it by the ratio of the solid's total surface area to the reactor's working volume. This adjustment results in a change in the reaction unit to mol per volume per unit time. When simplifying the above reactions, the reaction and reaction rate expressions become:

$$2A + 2B + 6C \rightarrow 2D + 3E \quad (7)$$

$$2B+3C \rightarrow G + 3E \quad (8)$$

Assuming the control is the chemical reaction, each component involved in the reaction has a corresponding differential equation. Thus, six simultaneous 1st-order differential equations (Eq. (9–13)) were derived with six known boundary conditions (initial values):

$$\frac{dC_A}{dt} = 2r_1 \quad (9)$$

Boundary condition t = 0; C_A = Initial concentration of NaOH (0.5; 1.0; 1.5; 2.0).

$$\frac{dC_B}{dt} = -2r_1 - 2r_2 \quad (10)$$

Boundary condition t = 0; C_B = 0 = NB; V = initial amount of alumina.

$$\frac{dC_C}{dt} = -6r_1 - 3r_2 \quad (11)$$

Boundary condition t = 0; C_C = initial amount of water.

$$\frac{dC_D}{dt} = 2r_1 \quad (12)$$

Boundary condition t = 0; C_D = 0 = initial concentration of $NaAl(OH)_4$.

$$\frac{dC_E}{dt} = 3r_1 + 3r_2 \quad (13)$$

Boundary condition t = 0; C_E = 0 = initial concentration of hydrogen.

Numerical solution. The differential equations were solved using the Runge-Kutta and the sum square error (SSE) methods [21]. Model fitting was performed for each data set, focusing on hydrogen gas production over time and the amount of Al_2O_3 solids at the end of the reaction. Initial guesses for reaction rate constants and reaction orders were used to minimize SSE.

Arrhenius equation. The reaction rate constants at each temperature were linearized to determine the Arrhenius equation for the two involved reactions. The results of the linearization provided the activation energy and collision factors for both reactions.

Mass transfer as rate limiting step. When mass transfer is the rate-limiting step, the surface reaction rate is assumed to be so fast that the concentration of the reactants (NaOH) at the surface is assumed to be zero. The reaction rate can be expressed in terms of the mass transfer equation (Eq. (14–16)).

$$\frac{dC_A}{dt} = -k_{ml} \cdot (C_A - C_{AS}) = -kml \cdot C_A \quad (14)$$

$$\frac{dn_B}{dt} = \frac{dC_A}{dt} \cdot V \cdot \left(1 + \frac{X_2}{X_1}\right) \quad (15)$$

$$\frac{dn_E}{dt} = \frac{-3}{2}\frac{dn_B}{dt} \quad (16)$$

where X_1 and X_2 are respectively the fractions of aluminum that follow reactions 1 and 2. The initial value of each equation is known and the calculation of the volume of hydrogen gas follows the ideal gas law. The

combination of Runge-Kutta and SSE is again used to calculate the mass transfer constant.

Surface reaction and mass transfer as rate limiting step. When calculating both steps that control the overall reaction rate, the pseudo-steady-state assumption is employed. The mass transfer rate is equal to the surface reaction rate. The β at Eq. (7) and γ at Eq. (8) are zero, which are used to simplify the equation. At this stage, two approaches are taken. First, the elementary reaction, α at Eq. (7) is 2. Second, α at Eq. (7) is 1. This approach is based on the calculation of the surface reaction as the controlling step, where α is approximately 1. When α at Eq. (7) is 2, the mass transfer rate and reaction rate of NaOH expressed in Eq. (17–20).

$$\frac{dC_A}{dt} = -k_{rl} \cdot C_{AS}^2 \quad (17)$$

$$\frac{dC_A}{dt} = -k_{ml} \cdot (C_A - C_{AS}) \quad (18)$$

$$k_{rl} \cdot C_{AS}^2 = -k_{ml} \cdot (C_A - C_{AS}) \quad (19)$$

$$C_{AS} = \frac{-k_{ml} + \sqrt{k_{ml}^2 - 4k_{rl}k_{ml}C_A}}{2k_{rl}} \quad (20)$$

The calculation is carried out in the following manner. All calculation procedures used in the controlled surface reaction calculations are used, but by substituting CA with CAs. When α at Eq. (7) is 1, the mass transfer rate and reaction rate of NaOH expressed in Eq. (21–24).

$$\frac{dC_A}{dt} = k_{rl} \cdot C_{AS} \quad (21)$$

$$\frac{dC_A}{dt} = -k_{ml} \cdot (C_A - C_{AS}) \quad (22)$$

$$-k_{rl} \cdot C_{AS} = -k_{ml} \cdot (C_A - C_{AS}) \quad (23)$$

$$C_{AS} = \frac{k_{ml}C_A}{(k_{rl} + k_{ml})} \quad (24)$$

■ RESULTS AND DISCUSSION

Li/Al LDHs Synthesis

The first stage of the reaction

Shrinking core model for heterogeneous solid-liquid reaction through five steps, namely: inter phases mass transfer, diffusion of liquid reactants through solid products to the core of unreacted solids, reaction of liquid reactants on the surface of unreacted solid reactants, diffusion of gas/liquid products through solid products, diffusion of gas/liquid products through the liquid film layer. Since the reaction, in this case, does not produce a porous product that encases the solid reactant core, the key factors influencing the reaction rate are interphase mass transfer and surface reactions. The reaction kinetics can be described by a model in which either a single stage governs the reaction rate or both stages contribute to its overall rate [22].

Surface reaction as rate limiting step

The hydrogen gas production during the initial reaction stage was monitored and recorded. Fig. 3. summarizes the results. The fastest reaction was achieved at 60 °C and a NaOH concentration of around 2 M. The reaction was completed in 1.6 min. In contrast, the slowest reaction occurred at a NaOH concentration of 0.5 M and a temperature of 30 °C, taking 25.9 min to complete. This demonstrates that both higher NaOH concentrations and elevated temperatures significantly reduce reaction time. This reaction rate is significantly faster than that observed with aluminum dross. Under the same conditions (2 M NaOH and 60 °C), the reaction with aluminum dross took 90 min [17]. The square aluminum foil waste with a thickness of 0.02 mm had a higher surface area than the 100 mesh aluminum dross. Even lower-purity aluminum dross required a longer reaction time, up to 4 h [23].

The second reaction produces hydrogen and solid black alumina. The percentage contribution of reaction (2) to the overall reaction can be calculated by separating and weighing the black solid from the reaction product solution immediately after the hydrogen formation reaction is complete. These data were used for kinetic model calculation, and Table 1. summarizes the contribution of reaction (2) to the total aluminum reaction. The findings show that the formation of aluminum oxide is minimal at low temperatures. However, when alumina is a by-product, this reaction is more efficient compared to other processes using dross, which can result in up to 17% alumina formation [17].

The findings from the implementation of the model, in which the surface reaction is assumed to be the rate-limiting step, are illustrated in Fig. 3. A close examination

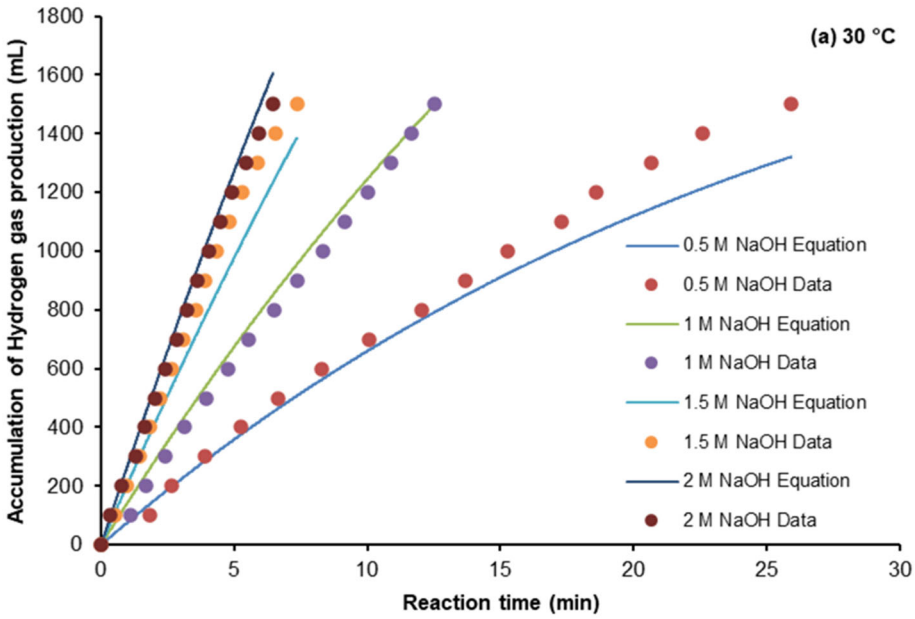
(a) 30 °C
Accumulation of Hydrogen gas production (mL)
Reaction time (min)
0.5 M NaOH Equation
0.5 M NaOH Data
1 M NaOH Equation
1 M NaOH Data
1.5 M NaOH Equation
1.5 M NaOH Data
2 M NaOH Equation
2 M NaOH Data

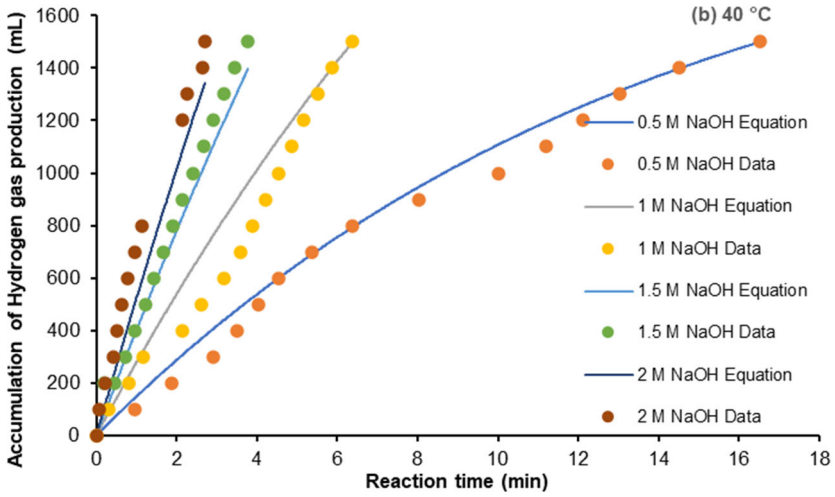
(b) 40 °C
Accumulation of Hydrogen gas production (mL)
Reaction time (min)
0.5 M NaOH Equation
0.5 M NaOH Data
1 M NaOH Equation
1 M NaOH Data
1.5 M NaOH Equation
1.5 M NaOH Data
2 M NaOH Equation
2 M NaOH Data

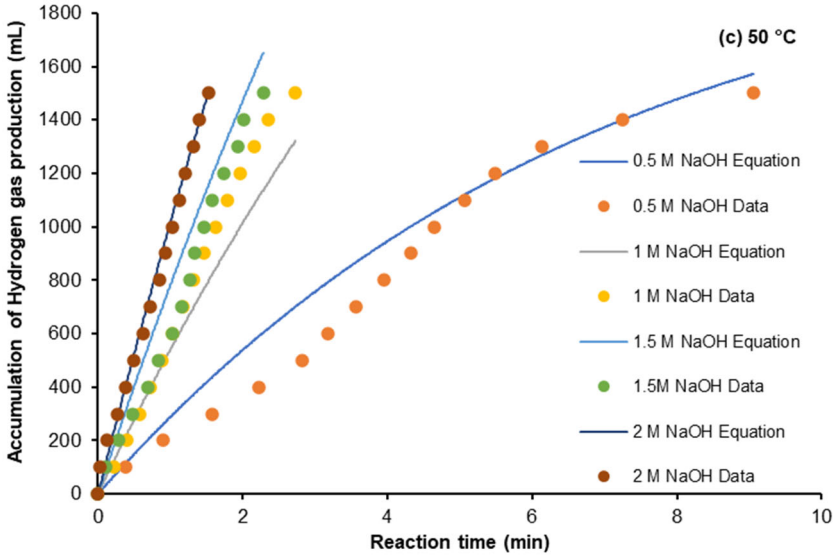
(c) 50 °C
Accumulation of Hydrogen gas production (mL)
Reaction time (min)
0.5 M NaOH Equation
0.5 M NaOH Data
1 M NaOH Equation
1 M NaOH Data
1.5 M NaOH Equation
1.5M NaOH Data
2 M NaOH Equation
2 M NaOH Data

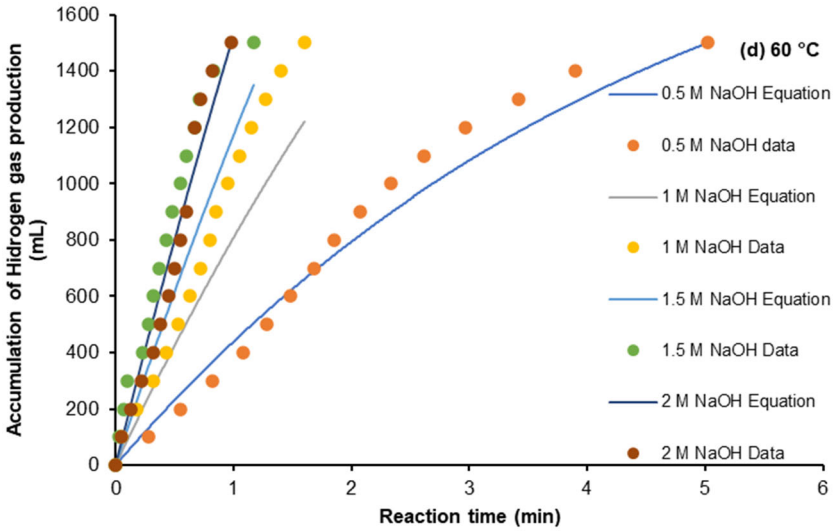

Fig 3. Data and fitting model isothermal first stage reaction at a varying temperature: (a) 30, (b) 40, (c) 50, and (d) 60 °C

Table 1. Percentage of aluminum oxide formation to total aluminum reaction

Concentration of NaOH solution (M)	Percentage of alumina formation (%)			
	30 °C	40 °C	50 °C	60 °C
0.5	2.15	3.12	0.90	3.63
1.0	2.21	0.48	1.96	4.37
1.5	1.53	0.53	0.11	4.50
2.0	0.16	0.90	2.01	6.85

of the data and calculation outcomes reveals minimal variations across all charts, suggesting a satisfactory alignment of the model with the data. Eq. (1) and (2) exhibit a constant reaction at each temperature. The calculated reaction constants and reaction orders are listed in Table 2. The reaction constant for Eq. (1) is considerably larger than that for Eq. (2), suggesting that Eq. (1) occurs at a faster rate. Consequently, the amount of Al_2O_3 produced by Eq. (2) in the final products is comparatively minimal.

The rate reaction constants were utilized to linearize the Arrhenius equation, with the results illustrated in Fig. 4. The collision factors and activation energies for both reactions are enumerated in Table 3. The linearization process yielded optimal fits, with R^2 values of 0.9946 and 0.9396 for Eq. (1) and (2), respectively,

Table 3. Activation energy and collision factors of first-step reactions

	E/R (K)	E (cal/mol)	Collision factor A
Eq. (7)	6188	12295.56	1.37×10^7
Eq. (8)	11977	23798.30	3.89×10^{12}

Table 2. Reaction constants and reaction order in hydrogen formation reactions

Reaction rate constant	Reaction temperature (K)			
	303	313	323	333
k_{1a}	0.0181	0.0355	0.0712	0.1104
k_{2a}	3.32×10^{-5}	8.40×10^{-5}	1.86×10^{-4}	1.36×10^{-3}
Reaction order				
α	0.9100			
β	0.0000			
γ	0.0000			

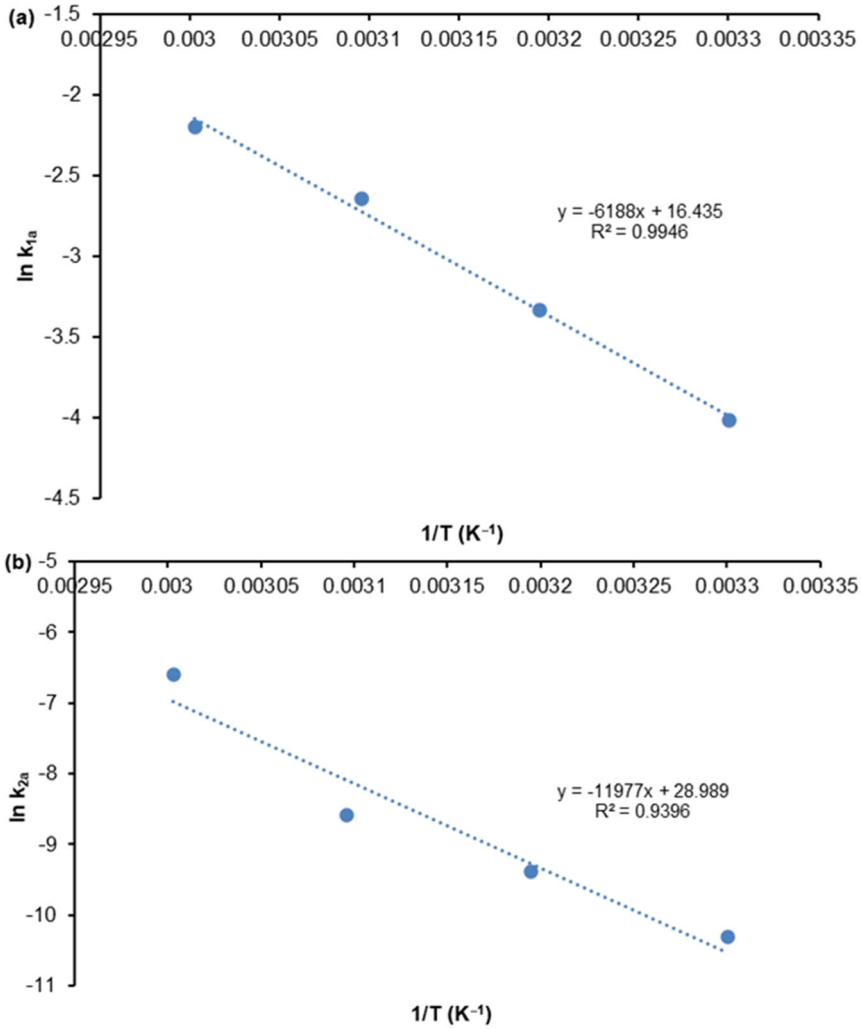

Fig 4. Linearization of Arrhenius for (a) Eq. (7) and (b) Eq. (8)

thereby substantiating the suitability of the Arrhenius correlation for both rate reaction constants. The activation energy for Eq. (2) is approximately double that of Eq. (1). The energy barrier for the second reaction is twice as high as that of the first reaction, which implies that the rate of the second reaction is lower than that of the first reaction. On the other hand, the Eq. (1) with lower activation energy has a higher reaction rate and is more efficient.

Mass transfer as rate limiting step

The mass transfer model as a rate-limiting step has been calculated and examined. Mass transfer coefficients at each isotherm reaction temperature were obtained from the kinetic modeling calculation and presented in Table 4. The mass transfer coefficients follow a polynomial empirical equation. The linearization result is presented in Fig. 5 with an R^2 value of 0.9998. The equations for the mass transfer are shown in Eq. (25).

Table 4. Mass transfer coefficients of NaOH

Temp [K]	303	313	323	333
$K_{ml}\left[\frac{1}{min}\right]$	0.036	0.071	0.135	0.244

$$k_{ml} = e^{-11.26}T^{20.292} \quad (25)$$

The most appropriate kinetic model can be determined based on the mean absolute percentage error (MAPE) values obtained for each tested model. Table 5 presents the MAPE results for the four models evaluated. The model in which mass transfer serves as the rate-limiting step exhibits the lowest MAPE value of 13.8%. This finding suggests that mass transfer between

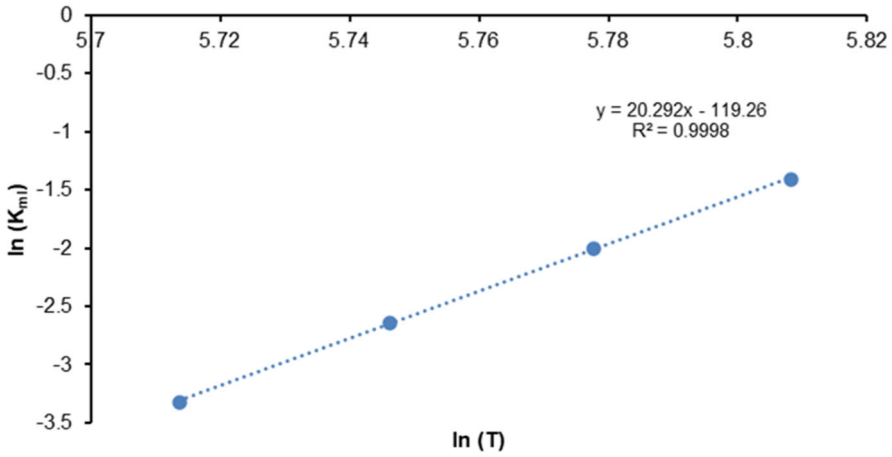

Fig 5. Linearization of mass transfer coefficients of NaOH

Table 5. MAPE of the first-stage reaction kinetic model

Temperature reaction (K)	Mean absolute percentage error (%)				
	303	313	323	333	Average
Surface reaction control step	8.87	14.54	14.26	19.34	14.30
Mass transfer control step	10.79	12.47	13.23	18.65	13.80
Both step control with reaction order 1	11.90	12.64	13.12	17.94	13.90
Both step control with reaction order 2	34.65	12.71	23.19	28.87	24.90

phases is the primary factor limiting the reaction rate.

Second stage reaction

As demonstrated in Fig. 6, the pH conditions for the formation of gibbsite and Li/Al-based crystals are delineated. The results indicate that the pH range for the formation of both crystals is between 11 and 12, with both crystals forming optimally at pH 11. This finding is consistent with other studies in which various LDHs have been synthesized at pH ranges of 8–12 [24-25]. However, it is noteworthy that Li/Al LDHs can also be synthesized at a lower pH of 5.5 [26-27].

The second-stage reaction between $NaAl(OH)_4$ and LiCl to produce Li/Al LDHs crystal was conducted under various pH and temperatures, and the results are

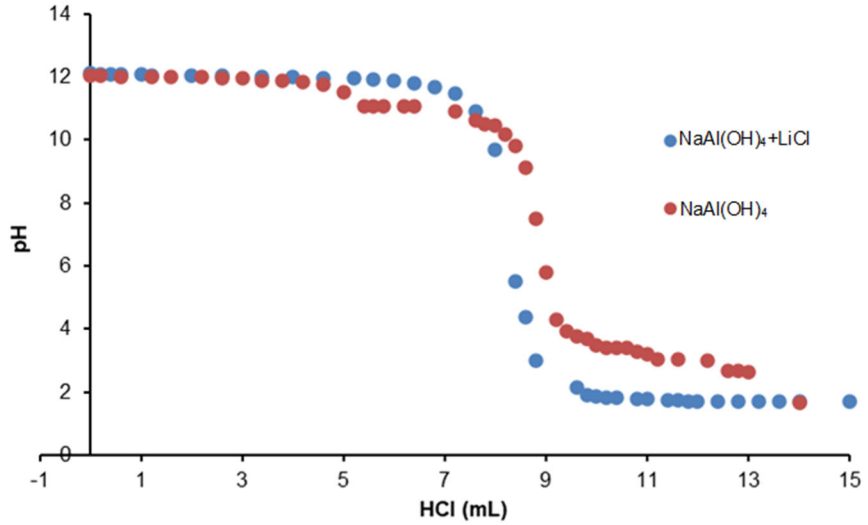

Fig 6. Titration curves of $NaAl(OH)_4$ and $NaAl(OH)_4$ + LiCl

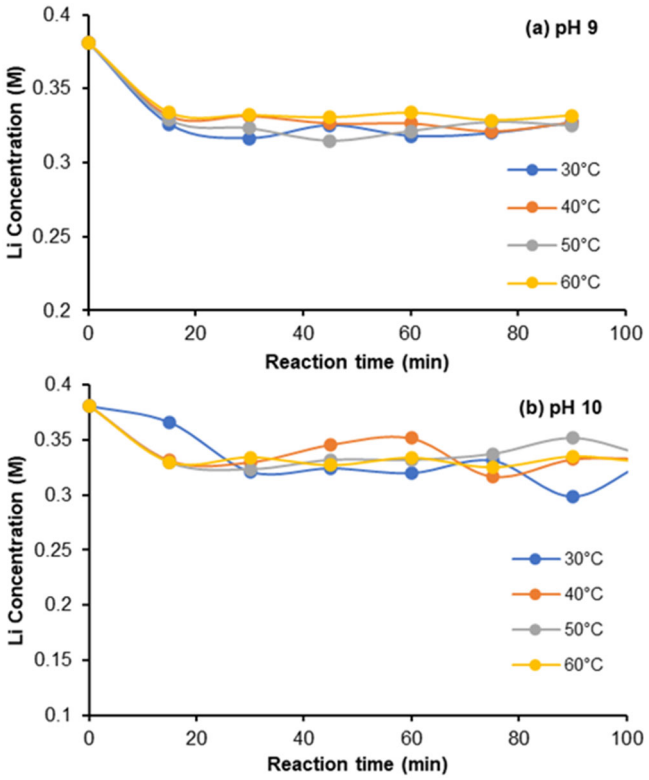

Fig 7. The impact of different temperature at (a) pH 9 and (b) pH 10 on the synthesis of $LiClAl_2(OH)_6$ crystals

presented in Fig. 7. The reduction in lithium reactants, which is an indication of the formation of the crystal adsorbent, occurred rapidly. It reached equilibrium in around 15 to 30 min at pH 10 and 9. The reaction time is notably faster than the intercalation of lithium ions into Gibbsite crystals, which requires around 1 h to reach equilibrium [16,28]. The reaction at pH 9 exhibits a faster equilibrium time because, at lower pH, the co-precipitation mechanism Eq. (6) is predominant in comparison to the intercalation mechanism Eq. (5). At the lowest temperatures, the reaction time to reach equilibrium is prolonged, but the yield is increased. In summary, the formation of the crystals from the mixture of $NaAl(OH)_4$ and LiCl solution follows a co-precipitation mechanism.

Characterization

The XRD analysis of aluminum waste, utilized as a raw material for synthesizing Li/Al LDHs, was executed using the Match software. The outcomes are displayed in Fig. 8. The analysis employed the COD-Inorg 2023.12.05 reference database with a peak-based search-match method. The XRD pattern exhibited peaks at 45°, 64°, and 78°, indicating that the material is composed entirely of aluminum, a finding consistent with other

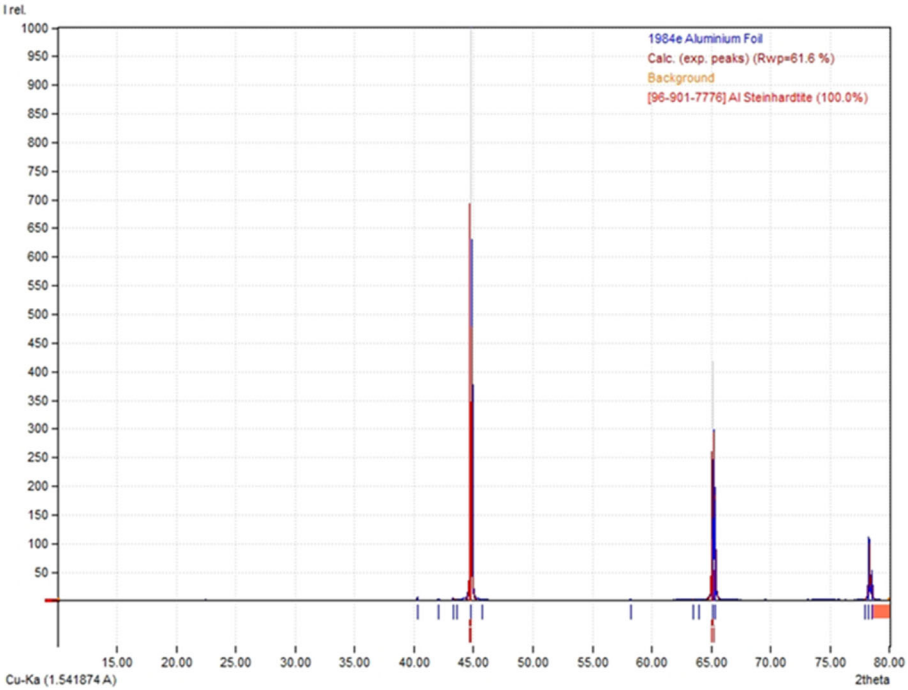

Fig 8. XRD pattern of aluminum waste

characterizations of aluminum [17,25-27]. The XRD results for gibbsite, lithium adsorbent, and activated lithium adsorbent are presented in Fig. 9.

Al(OH)$_3$ (gibbsite)

The blue XRD pattern corresponds to pure gibbsite, with characteristic peaks marked with asterisks (*) at 2θ values of 18.7°, 20.3°, 27.8°, 53.2°, and 63.6°. These peaks show the presence of crystalline Al(OH)$_3$, which is a crystalline substance [29-30].

Li/Al LDHs crystal

The red XRD pattern corresponds to the synthesized Li/Al LDH adsorbent. Peaks at 11.6°, 20.3°, 23.1°, 36.1°, 40°, 47.5°, 54°, 57°, 63°, and 64° confirm the presence of $LiAl_2(OH)_6Cl{\cdot}xH_2O$, indicative of a well-ordered LDH structure [31-34]. Peaks marked with triangles (Δ) are characteristic of the crystal phase, indicating the formation of the LDH structure [35-36].

Activated Li/Al LDH

The black XRD pattern corresponds to the activated Li/Al LDHs adsorbent after partial lithium deintercalation. The presence of peaks with asterisks and triangles represents the presence of the gibbsite and the double-layer structure. The heightened intensity of gibbsite peaks (marked with *) suggests that the activation process, involving lithium deintercalation, results in a partial transformation of the LDHs structure into gibbsite. The formation of these peaks represents the successful synthesis of $LiCl\text{-}Al_2OH_6{\cdot}xH_2O$ with the expected layered structure.

The characterization of the white adsorbent powder was performed using FTIR, with the results displayed in Fig. 10. The presence of an absorption band measuring 3462 cm^{-1} is indicative of O–H stretching vibrations. The broadness of the peak signifies the presence of strong hydrogen bonds within the compound. This is a typical feature of layered structures, where water molecules are constantly intercalated [19,30-31,35]. The band around 1628 cm^{-1} is caused by O–H groups' bending vibrations. This phenomenon indicates that water molecules are located in the LDH's interlayer spaces. These molecules then form hydrogen bonds by coordinating with metal cations [30-31,36].

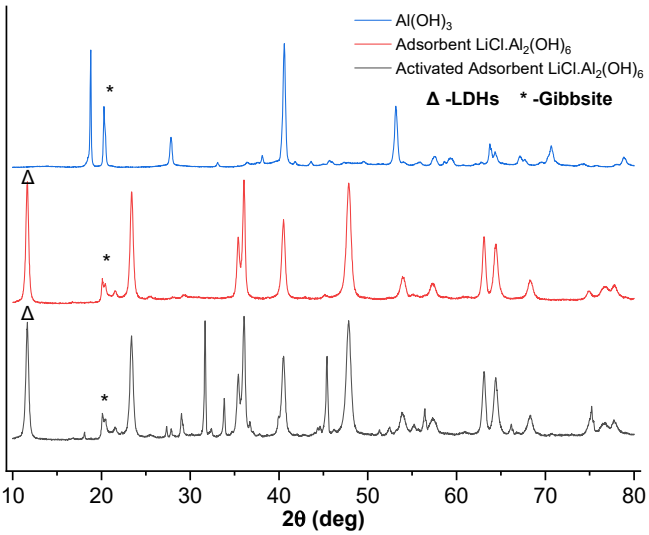

Fig 9. Combine XRD pattern of (a) Al(OH)$_3$, (b) Li/Al LDH adsorbent, and (c) activated Li/Al LDH adsorbent

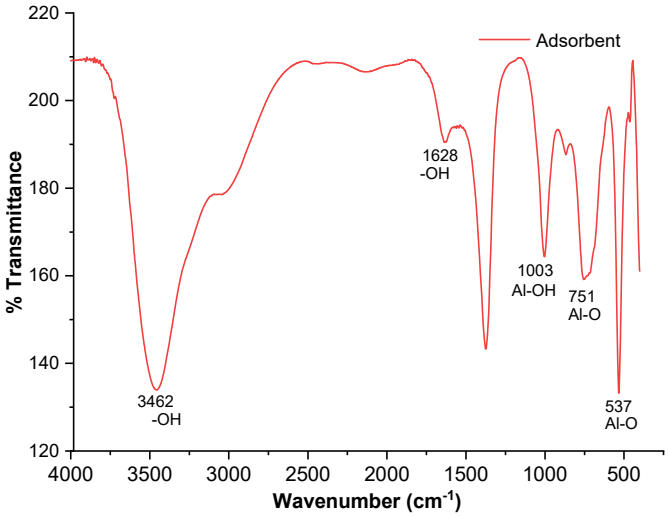

Fig 10. FTIR spectra Li/Al LDH adsorbent

The peak observed at 1003 cm^{-1} is indicative of Al–OH bending vibrations, thereby confirming the presence of Al(OH)$_3$ within the structure. This finding is in alignment with the Li/Al LDH structure, wherein aluminum is present in the hydroxide layers [36]. Al–O vibrations are indicated by additional peaks at 751 and 537 cm^{-1}. The presence of aluminum oxide or hydroxide components in the structure is confirmed by the peak at 751 cm^{-1}, which further substantiates the existence of aluminum in the crystal [19,30-31,35]. The peak of 537 cm^{-1} is the same as the different Al–O bonding modes found in the structures of Li/Al LDHs [30,35].

The FTIR spectrum confirms the presence of hydroxyl groups, both free and intercalated water molecules, and Al–O bonds within the adsorbent. The broad O–H stretching and bending vibrations indicate a hydrated structure characteristic of LDHs.

Li/Al LDHs Performance

As demonstrated in Fig. 11, the adsorbent derived from aluminum foil waste exhibits a higher adsorption capacity with increasing lithium concentrations in the brine. The maximum adsorption capacity reached 6.7 mg Li/g adsorbent, at 1350 ppm lithium and 0.25 M $MgCl_2$. At equilibrium, the remaining lithium concentration was 730 ppm. Comparative studies demonstrate that Li/Al LDH commercial has 5.9 mg Li/g adsorbent [16], and typically exhibits an adsorption capacity ranging from 3.0 to 6.3 mg Li/g adsorbent, although some studies report higher capacities up to 10 mg Li/g adsorbent [37-41]. This finding underscores the competitive performance of the adsorbent derived from aluminum foil waste when benchmarked against commercial adsorbents. At 39 ppm lithium, the Li/Al LDH adsorbent exhibited an adsorption capacity of 0.2 mg Li/g with a 25.6% recovery rate, highlighting its potential for brines with higher lithium concentrations, particularly in Indonesia. However, this technology is not suitable for low-concentration geothermal brines. Pre-concentration methods, such as reverse osmosis or evaporation, are required before application [10].

A multitude of adsorption equilibrium equations were utilized to calibrate the model, with the most optimal outcomes depicted in Fig. 12. The coefficient of determination for the Freundlich equation is 0.8315, suggesting that adsorption occurs under heterogeneous and multi-layer conditions. This observation is in accordance with other studies that have substantiated the applicability of the Freundlich model for Li/Al LDHs adsorbents [32]. Fitting the experimental data to the Langmuir equation yielded a Langmuir constant of 328.014 L/mg. The Gibbs free energy (ΔG) was calculated using $\Delta G = -RT\ln Ka$, resulting in −14.594 kJ/mol at 303 K. The commercial product has Gibbs free energy in the range 10.720 to −8.440 kJ/mol [16]. The negative ΔG confirms that the adsorption process is spontaneous and thermodynamically favorable. Its moderate magnitude suggests physisorption, driven by weak van der Waals or electrostatic interactions. This adsorption mechanism is relatively weak but effective since physisorption typically falls within −20 to 0 kJ/mol. The spontaneity implies natural adsorbate removal without external energy input, enhancing its practicality. Further temperature studies could provide insights into enthalpy (ΔH) and entropy (ΔS), optimizing adsorption efficiency.

An investigation was conducted to examine how $MgCl_2$ concentration influences the adsorbent. The findings, presented in Table 6, demonstrate that higher $MgCl_2$ concentrations result in increased adsorption capacity. This enhancement can be attributed to the

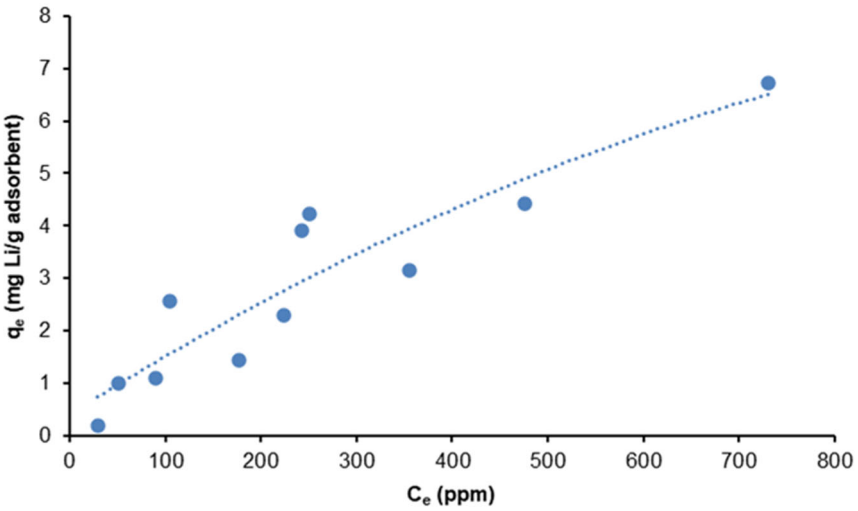

Fig 11. Adsorption capacity of $LiClAl_2(OH)_6$ adsorbent in L/S 20 adsorption operation at 30 °C

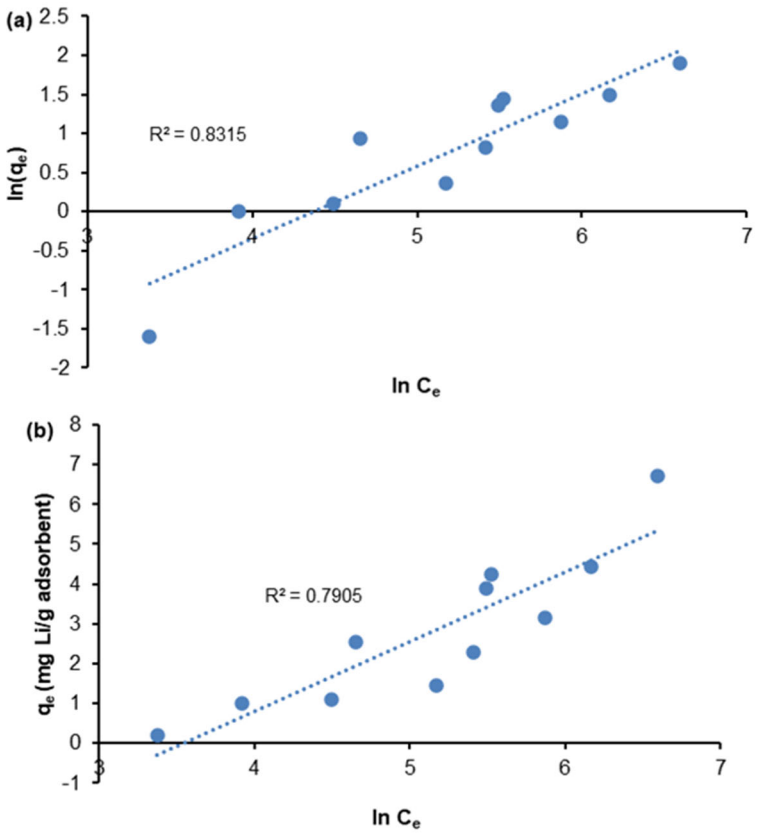

Fig 12. Fitting curve of linearization of (a) Freundlich and (b) Temkin equations

Table 6. Effect of $MgCl_2$ concentration in brine on adsorbent performance

$MgCl_2$ concentration (M)	0	0.5	1.0	2.0
Adsorption capacity (mg Li/g adsorbent)	2.998	3.716	4.127	4.52

Table 7. Summarizes the adsorbent quality and synthesis method

No.	Parameter	Recent research	Previous research	Ref
1	Raw material	Aluminum waste	Analytical grade chemical	[11]
2	Synthesis method	Double stage	Direct precipitation	[11]
3	pH of raw material	Base	Acid	[11,16]
4	Max adsorption capacity (mg Li/g adsorbent)	6.7	5.9	[16]
5	The most proper isotherm adsorption curve	Freundlich	Freundlich, Sips, Langmuir	[16,42]
6	Minimum concentration of lithium in brine (ppm)	39	350	[16]
7	Gibbs free energy (kJ/mol)	−14.594	−10.72 to −8.44	[16]

presence of Cl^- ions, which function as structural pillars within the crystal, thereby facilitating the entry of lithium ions into the crystal structure [16]. Table 7 summarizes the adsorbent quality and synthesis method used in this study, along with a comparison to previous research. The results show that this study utilizes more cost-effective and environmentally friendly raw materials. Despite this, the adsorbent's performance remains competitive with those produced using analytical-grade and commercial LDHs adsorbents in prior studies.

■ CONCLUSION

The synthesis of Li/Al LDHs from aluminum waste was successfully achieved through a two-step reaction.

The reaction kinetics and co-precipitation process were thoroughly studied. The product was characterized using XRD and FTIR. The findings indicate that the adsorbent demonstrated a notable capacity for lithium-ion adsorption, with a 6.7 mg Li/g adsorbent size. The FTIR and XRD data confirmed the crystal structure's well-ordered composition. An evaluation was conducted of the adsorption performance of the lithium adsorbent under a variety of conditions, including different concentrations of lithium and $MgCl_2$. The data regarding the adsorbent's effectiveness were obtained using the Freundlich equation. This study contributes to the advancement of sustainable technologies for lithium extraction by leveraging aluminum waste as a primary raw material. The findings of this research hold significant promise in enhancing the efficiency and environmental sustainability of lithium recovery processes in diverse industrial contexts.

■ ACKNOWLEDGMENTS

A grant scheme "*Penelitian Disertasi Doktor*" No: 1930/UN1/DITLIT/Dit-Lit/PT.01.03/2022 from "*Direktorat Pendidikan Tinggi, Riset dan Teknologi, Kementrian Pendidikan, Kebudayaan, Riset dan Teknologi Indonesia*" supported this research and paper.

■ CONFLICT OF INTEREST

The authors hereby affirm that there are no conflicts of interest to disclose. All authors have reviewed and approved the manuscript's content, and no financial interests are involved.

■ AUTHOR CONTRIBUTIONS

Salafudin conducted the experiment and performed the data analysis, and he was responsible for all calculations. Salafudin, Agus Prasetya, I Wayan Warmada, and Tri Bayu Murti Petrus collaboratively wrote and revised the manuscript. The research was overseen by Tri Bayu Murti Petrus, Agus Prasetya, and I Wayan Warmada, who all provided their consent for the final version of this manuscript.

■ REFERENCES

[1] Abbasi, K.R., Shahbaz, M., Zhang, J., Irfan, M., and Alvarado, R., 2022, Analyze the environmental sustainability factors of China: The role of fossil fuel energy and renewable energy, *Renewable Energy*, 187, 390–402.

[2] Salehi, M., 2022, Global water shortage and potable water safety; Today's concern and tomorrow's crisis, *Environ. Int.*, 158, 106936.

[3] Razmjoo, A., Gakenia Kaigutha, L., Vaziri Rad, M.A., Marzband, M., Davarpanah, A., and Denai, M., 2021, A Technical analysis investigating energy sustainability utilizing reliable renewable energy sources to reduce CO_2 emissions in a high potential area, *Renewable Energy*, 164, 46–57.

[4] Huang, T.Y., Pérez-Cardona, J.R., Zhao, F., Sutherland, J.W., and Paranthaman, M.P., 2021, Life cycle assessment and techno-economic assessment of lithium recovery from geothermal brine, *ACS Sustainable Chem. Eng.*, 9 (19), 6551–6560.

[5] Flexer, V., Baspineiro, C.F., and Galli, C.I., 2018, Lithium recovery from brines: A vital raw material for green energies with a potential environmental impact in its mining and processing, *Sci. Total Environ.*, 639, 1188–1204.

[6] Zhang, X., Han, A., and Yang, Y., 2020, Review on the production of high-purity lithium metal, *J. Mater. Chem. A*, 8 (43), 22455–22466.

[7] Murphy, O., and Haji, M.N., 2022, A review of technologies for direct lithium extraction from low Li^+ concentration aqueous solutions, *Front. Chem. Eng.*, 4, 1008680.

[8] Tangkas, I.W.C.W.H., Sujoto, V.S.H., Astuti, W., Jenie, S.N.A., Anggara, F., Utama, A.P., Petrus, H.T.B.M., and Sutijan, S., 2023, Synthesis of titanium ion sieves and its application for lithium recovery from artificial Indonesian geothermal brine, *J. Sustainable Metall.*, 9 (2), 613–624.

[9] Walanda, D.K., 2007, Kinetics transformation of spinel type $LiMn_2O_4$ into tunnel type MnO_2, *Indones. J. Chem.*, 7 (2), 117–120.

[10] Sulistiyono, E., Lalasari, L.H., Mayangsari, W., and Prasetyo, A.B., 2018, Study of lithium extraction from brine water, Bledug Kuwu, Indonesia by the precipitation series of oxalic acid and carbonate sodium, *AIP Conf. Proc.*, 1964, 020007.

[11] Wu, L., Li, L., Evans, S.F., Eskander, T.A., Moyer, B.A., Hu, Z., Antonick, P.J., Harrison, S., Paranthaman, M.P., Riman, R., and Navrotsky, A., 2019, Lithium aluminum-layered double hydroxide chlorides (LDH): Formation enthalpies and energetics for lithium ion capture, *J. Am. Ceram. Soc.*, 102 (5), 2398–2404.

[12] Stringfellow, W.T., and Dobson, P.F., 2021, Technology for the recovery of lithium from geothermal brines, *Energies*, 14 (20), 6805.

[13] Li, X., Mo, Y., Qing, W., Shao, S., Tang, C.Y., and Li, J., 2019, Membrane-based technologies for lithium recovery from water lithium resources: A review, *J. Membr. Sci.*, 591, 117317.

[14] Sun, Y., Yun, R., Zang, Y., Pu, M., and Xiang, X., 2019, Highly Efficient lithium recovery from pre-synthesized chlorine-ion-intercalated LiAl-layered double hydroxides via a mild solution chemistry process, *Materials*, 12 (12), 1968.

[15] Jiang, H., Zhang, S., Yang, Y., and Yu, J., 2020, Synergic and competitive adsorption of Li–Na–$MgCl_2$ onto lithium–aluminum hydroxides, *Adsorption*, 26 (7), 1039–1049.

[16] Graham, T.R., Hu, J.Z., Zhang, X., Dembowski, M., Jaegers, N.R., Wan, C., Bowden, M., Lipton, A.S., Felmy, A.R., Clark, S.B., Rosso, K.M., and Pearce, C.I., 2019, Unraveling gibbsite transformation pathways into LiAl-LDH in concentrated lithium hydroxide, *Inorg. Chem.*, 58 (18), 12385–12394.

[17] Meshram, A., Jain, A., Rao, M.D., and Singh, K.K., 2019, From industrial waste to valuable products: preparation of hydrogen gas and alumina from aluminium dross, *J. Mater. Cycles Waste Manage.*, 21 (4), 984–993.

[18] Dembowski, M., Snyder, M.M., Delegard, C.H., Reynolds, J.G., Graham, T.R., Wang, H.W., Leavy, I.I., Baum, S.R., Qafoku, O., Fountain, M.S., Rosso, K.M., Clark, S.B., and Pearce, C.I., 2019, Ion–ion interactions enhance aluminum solubility in alkaline suspensions of nano-gibbsite (α-$Al(OH)_3$) with sodium nitrite/nitrate, *Phys. Chem. Chem. Phys.*, 22 (8), 4368–4378.

[19] Supriadi, H., Trisnawati, I., Handini, T., Susilowati, S.R., Sujoto, V.S.H., Mulyono, P., and Petrus, H.T.B.M., 2023, Kinetics study of yttrium leaching from zircon tailings using sulfuric acid, *Indones. J. Chem.*, 23 (2), 489–498.

[20] Fadhilah, N., Muharja, M., Risanti, D.D., Wahyuono, R.A., Satrio, D., Khamil, A.I., and Fadilah, S.N., 2023, Kinetic study of the aluminum–water reaction using NaOH/$NaAlO_2$ catalyst for hydrogen production from aluminum cans waste, *Bull. Chem. React. Eng. Catal.*, 18 (4), 615–626.

[21] Madhukesh, J.K., Naveen Kumar, R., Punith Gowda, R.J., Prasannakumara, B.C., Ramesh, G.K., Ijaz Khan, M., Ullah Khan, S., and Chu, Y.M., 2021, Numerical simulation of AA7072-AA7075/water-based hybrid nanofluid flow over a curved stretching sheet with Newtonian heating: A non-Fourier heat flux model approach, *J. Mol. Liq.*, 335, 116103.

[22] Mezulis, A., Richter, C., Lesnicenoks, P., Knoks, A., Varnagiris, S., Urbonavicius, M., Milcius, D., and Kleperis, J., 2023, Studies on water–aluminum scrap reaction kinetics in two steps and the efficiency of green hydrogen production, *Energies*, 16 (14), 5554.

[23] Wajima, T., 2020, A novel process for recycling of aluminum dross using alkali fusion, *Mater. Trans.*, 61 (11), 2208–2215.

[24] Murayama, N., Maekawa, I., Ushiro, H., Miyoshi, T., Shibata, J., and Valix, M., 2012, Synthesis of various layered double hydroxides using aluminum dross generated in aluminum recycling process, *Int. J. Miner. Process.*, 110-111, 46–52.

[25] Cai, J., Zhao, X., Zhang, Y., Zhang, Q., and Pan, B., 2018, Enhanced fluoride removal by La-doped Li/Al layered double hydroxides, *J. Colloid Interface Sci.*, 509, 353–359.

[26] Wu, L., Evans, S.F., Cheng, Y., Navrotsky, A., Moyer, B.A., Harrison, S., and Paranthaman, M.P., 2019, Neutron spectroscopic and thermochemical characterization of lithium-aluminum-layered double hydroxide chloride: Implications for lithium recovery, *J. Phys. Chem. C*, 123 (34), 20723–20729.

[27] Liu, G., Zhu, Z., Zhao, N., Fang, Y., Gao, Y., Zhu, Y., and Zhang, L., 2020, Mn-Fe layered double hydroxide intercalated with ethylene-diaminetetraacetate anion: Synthesis and removal of As(III) from aqueous solution around pH 2–11, *Int. J. Environ. Res. Public Health*, 17 (24), 9341.

[28] Wimpenny, J., Colla, C.A., Yu, P., Yin, Q.Z., Rustad, J.R., and Casey, W.H., 2015, Lithium isotope fractionation during uptake by gibbsite, *Geochim. Cosmochim. Acta*, 168, 133–150.

[29] Simonnet, T., Grangeon, S., Claret, F., Maubec, N., Fall, M.D., Harba, R., and Galerne, B., 2024, Phase quantification using deep neural network processing of XRD patterns, *IUCrJ*, 11 (Pt. 5), 859–870.

[30] Zolfaghari, R., Rezai, B., Bahri, Z., and Mahmoudian, M., 2020, Influences of new synthesized active seeds and industrial seed on the aluminum hydroxide precipitation from sodium aluminate solution, *J. Sustainable Metall.*, 6 (4), 643–658.

[31] Fogg, A.M., Freij, A.J., and Parkinson, G.M., 2002, Synthesis and anion exchange chemistry of rhombohedral Li/Al layered double hydroxides, *Chem. Mater.*, 14 (1), 232–234.

[32] Zhong, J., Lin, S., and Yu, J., 2021, Lithium recovery from ultrahigh Mg^{2+}/Li^{+} ratio brine using a novel granulated Li/Al-LDHs adsorbent, *Sep. Purif. Technol.*, 256, 117780.

[33] Zhong, J., Lin, S., and Yu, J., 2020, Effects of excessive lithium deintercalation on Li^{+} adsorption performance and structural stability of lithium/aluminum layered double hydroxides, *J. Colloid Interface Sci.*, 572, 107–113.

[34] Liu, J., Li, Y., Huang, X., Li, G., and Li, Z., 2008, Layered double hydroxide nano- and microstructures grown directly on metal substrates and their calcined products for application as Li-ion battery electrodes, *Adv. Funct. Mater.*, 18 (9), 1448–1458.

[35] Paranthaman, M.P., Li, L., Luo, J., Hoke, T., Ucar, H., Moyer, B.A., and Harrison, S., 2017, Recovery of lithium from geothermal brine with lithium-aluminum layered double hydroxide chloride sorbents, *Environ. Sci. Technol.*, 51 (22), 13481–13486.

[36] Zhang, Y., Liu, J., Li, Y., Yu, M., Li, S.M., and Xue, B., 2015, Fabrication of inhibitor anion-intercalated layered double hydroxide host films on aluminum alloy 2024 and their anticorrosion properties, *J. Coat. Technol. Res.*, 12 (2), 293–302.

[37] Chen, Y.J., and Uan, J.Y., 2023, The effect of lithium ion leaching from calcined Li–Al hydrotalcite on the rapid removal of Ni^{2+}/Cu^{2+} from contaminated aqueous solutions, *Nanomaterials*, 13 (9), 1477.

[38] Jiang, H., Yang Y., Sun, S., and Yu, J., 2020, Adsorption of lithium ions on lithium-aluminum hydroxides: Equilibrium and kinetics, *Can. J. Chem. Eng.*, 98 (2), 544–555.

Yang, Y., Jiang, H., and Yu, J., 2022, Investigation on desorption process in fixed bed for lithium recovery, *Sep. Purif. Technol.*, 281, 119596.

[39] Lv, S., Zhao, Y., Zhang, L., Zhang, T., Dong, G., Li, D., Cheng, S., Ma, S., Song, S., Quintana, M., 2023, Anion regulation strategy of lithium-aluminum layered double hydroxides for strengthening resistance to deactivation in lithium recovery from brines, *Chem. Eng. J.*, 472, 145026.

[40] Zhong, J., Lin, S., and Yu, J., 2021, Li^{+} adsorption performance and mechanism using lithium/aluminum layered double hydroxides in low grade brines, *Desalination*, 505, 114983.

[41] Luo, Q., Dong, M., Li, Q., Wu, Z., Liu, Z., and Li, J., 2022, Improve the durability of lithium adsorbent Li/Al-LDHs by Fe^{3+} substitution and nanocomposite of FeOOH, *Miner. Eng.*, 185, 107717.